FRONTIERS OF PHYSICS

RESEARCH ARTICLE
Volume 21 / Issue 9 / 095207 / 2026

Quantum-squeezing-induced critical non-Hermitian skin effects with $\mathbb{Z}_2$ skin modes

Yu-Wen Liang*, Zhao-Fan Cai*, Tao Liu†, Xiaoming Wei‡

School of Physics and Optoelectronics, South China University of Technology, Guangzhou 510640, China
*These authors contributed equally to this work.
Corresponding authors. E-mail: †liutao0716@scut.edu.cn, ‡xmwei@scut.edu.cn
Received April 10, 2026; accepted April 16, 2026

ABSTRACT

Previous studies of the critical non-Hermitian skin effect (cNHSE) have mainly focused on explicitly coupled non-Hermitian chains with different decay lengths, where skin modes localize at opposite boundaries. Here, we show that a cNHSE can instead emerge in a Hermitian bosonic quadratic ladder composed of identical chains, each of which already exhibits a $\mathbb{Z}_2$ skin effect in the decoupled limit. Within the Bogoliubov–de Gennes framework, the bosonic excitation spectrum becomes intrinsically non-Hermitian and features a symmetry-protected fourfold degeneracy with opposite spectral windings. By separating the degenerate sectors via a unitary transformation, we find that even an infinitesimal interchain coupling triggers a cNHSE, causing a discontinuous transition from real to complex spectra in the thermodynamic limit. In finite systems, this leads to scale-free localization and size-dependent dynamical instability, where the simple $\mathbb{Z}_2$-type pairing structure of the decoupled chains breaks down. Introducing staggered squeezing breaks inversion symmetry, lifts the degeneracy, and induces a size-dependent skin transition across distinct point-gap phases, markedly enhancing boundary localization. These findings establish Hermitian squeezed-boson lattices as practical, experimentally accessible platforms for realizing and controlling cNHSE without the need for dissipative engineering.

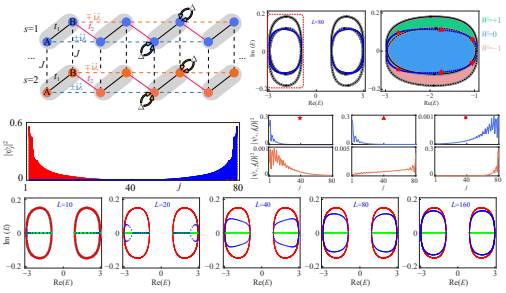

Keywords non-Hermitian skin effect, quantum squeezing

1 Introduction

Recent interest in non-Hermitian systems stems from their ability to host novel phenomena unattainable in their Hermitian counterparts [1–35]. Among these phenomena,the non-Hermitian skin effect (NHSE) is particularly striking, with a macroscopic number of eigenstates becoming localized at the boundaries of lattices [36–72], resulting in markedly different energy spectra under open and periodic boundary conditions (OBCs and PBCs). This spectral sensitivity reflects the breakdown of the conventional bulk–boundary correspondence, which can be restored using the non-Bloch band theory, formulated in terms of the generalized Brillouin zone (GBZ) with complexified momentum [36–38, 73].

More recently, it has been shown that coupling non-Hermitian chains with opposite NHSE decay lengths can give rise to a critical non-Hermitian skin effect (cNHSE) [74–87], characterized by discontinuous jumps of both eigenvalues and eigenstates across a critical point in the thermodynamic limit. In finite-size systems, however, the OBC spectrum remains continuous under small variations, and the eigenstates display scale-free localization,

https://doi.org/10.15302/frontphys.2026.095207

with a localization length proportional to the system size. These features are well captured both numerically [74] and analytically [77, 79] within the GBZ framework. In addition, related coupled-chain studies have reported pseudo-mobility edges and hybrid localization behaviors [83, 84], as well as system-size-dependent boundary modes and anomalous scaling near critical regimes [85–87]. The cNHSE has been further explored in a single closed chain [88], two-dimensional systems with boundary defects [89], and many-body settings [90]. Despite these advances, the cNHSE has been studied primarily in systems of coupled chains where each individual chain exhibits the NHSE with skin modes localized at opposite boundaries. An important and fundamentally different scenario, namely, coupled chains in which each chain hosts a $\mathbb{Z}_2$ skin effect in the decoupled limit, with skin modes simultaneously localized at both boundaries, has received little attention so far. Whether and how the cNHSE manifests in this setting therefore remains largely unexplored.

Non-Hermitian systems, which typically involve gain, loss, or other effective non-conservative dynamics, have been extensively studied in both classical and quantum platforms, often through engineered couplings to dissipative baths [1]. A central challenge in quantum settings is the need to post-select trajectories without quantum jumps [91, 92]. Since quantum jumps occur stochastically, the probability of observing a no-jump trajectory decays exponentially with time, making the study of long-time dynamics experimentally challenging [93]. These limitations motivate the use of Hermitian bosonic quadratic systems, in which effective non-Hermitian behavior arises naturally from the equations of motion [94–110]. In these systems, dynamics remain fully coherent, eliminating the need for post-selection and providing a robust, experimentally accessible platform for probing non-Hermitian phenomena. This naturally raises the question of whether a cNHSE can arise in coupled Hermitian bosonic quadratic lattices, where each individual chain exhibits a $\mathbb{Z}_2$ skin effect in the decoupled limit, in contrast to previously studied scenarios.

In this study, we construct a Hermitian bosonic quadratic Hamiltonian in a ladder of two identical legs with onsite quantum squeezing. Within the Bogoliubov–de Gennes framework, the many-body dynamics map to an effective single-particle non-Hermitian dynamical matrix, whose quasiparticle spectrum exhibits a fourfold degeneracy protected by particle–hole, inversion, and mirror symmetries. By applying a unitary transformation to separate the degenerate sectors, we show that an infinitesimal interchain coupling induces a quantum-squeezing-driven cNHSE: in the thermodynamic limit, the spectrum undergoes a discontinuous jump, while finite systems exhibit scale-free localization and size-dependent dynamical instability, where the simple $\mathbb{Z}_2$-type pairing structure of the decoupled chains breaks down. Importantly, this instability exhibits a size-controlled onset, rather than being solely determined by system parameters, providing a mechanism to tune its emergence and strength via system size, in contrast to conventional non-Hermitian systems with explicit gain and loss. Introducing staggered squeezing breaks inversion symmetry, lifts the degeneracy, and drives a size-dependent skin transition across topologically distinct point-gap phases, strongly enhancing boundary localization. Importantly, unlike conventional coupled non-Hermitian chain models where all eigenmodes share a uniform decay length, the present system exhibits intrinsically energy-dependent localization even at the single-chain level, such that no single characteristic localization length can be defined.

The paper is organized as follows. In Section 2, we construct a one-dimensional bosonic ladder system composed of two identical, coupled Su–Schrieffer–Heeger chains that include next-nearest-neighbor hopping and onsite quantum squeezing. Within the Bogoliubov–de Gennes framework, we derive the dynamical matrix of the quantum-squeezed system and analyze its symmetry properties. In Section 3, we demonstrate the cNHSE in Hermitian bosonic quadratic lattices, where each individual chain already supports a $\mathbb{Z}_2$ skin effect in the decoupled limit, which is fundamentally distinct from previously studied cNHSE scenarios. We further show that the system exhibits size-dependent dynamical instability. In Section 4, we introduce a staggered onsite squeezing perturbation, which breaks inversion symmetry and lifts the associated degeneracy. Moreover, this perturbation induces a size-dependent skin transition and enhances boundary localization. Finally, Section 5 summarizes the paper.

2 Model

We consider a one-dimensional (1D) bosonic ladder system composed of two identical, coupled Su–Schrieffer–Heeger (SSH) chains that include next-nearest-neighbor hopping and onsite quantum squeezing for bosons, as illustrated in Fig. 1(a). The real-space Hamiltonian of the system is given by

$$\begin{aligned}\hat{H} = &\sum_{s=1,2}\sum_{j=1}^{L}\Big(t_1\hat{a}_{j,s}^{\dagger}\hat{b}_{j,s} + t_2\hat{a}_{j+1,s}^{\dagger}\hat{b}_{j,s} + \mathrm{i}\lambda\hat{a}_{j+1,s}^{\dagger}\hat{a}_{j,s} \\ &+ \mathrm{i}\lambda\hat{b}_{j,s}^{\dagger}\hat{b}_{j+1,s} + \frac{\Delta}{2}\hat{a}_{j,s}^{\dagger}\hat{a}_{j,s}^{\dagger} + \frac{\Delta}{2}\hat{b}_{j,s}^{\dagger}\hat{b}_{j,s}^{\dagger} + \mathrm{H.c.}\Big) \\ &+ J\sum_{j=1}^{L}\left(\hat{a}_{j,1}^{\dagger}\hat{a}_{j,2} + \hat{b}_{j,1}^{\dagger}\hat{b}_{j,2} + \mathrm{H.c.}\right),\end{aligned} \tag{1}$$

where $\hat{a}_{j,s}$ and $\hat{b}_{j,s}$ annihilate bosons on sublattices A

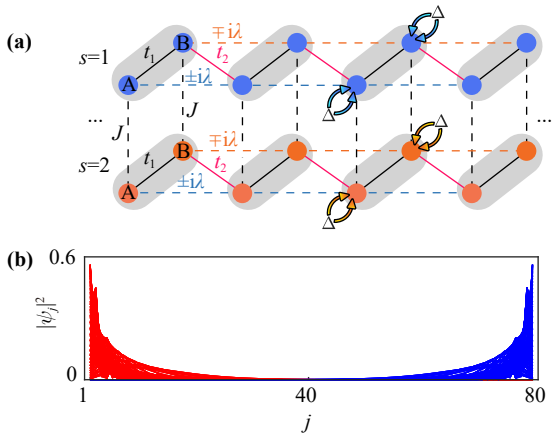

Fig. 1 **(a)** Schematic of a one-dimensional quadratic bosonic Hermitian ladder lattice composed of two identical SSH-type chains. The parameters t_1 and t_2 represent the intracell and intercell hopping amplitudes, respectively, λ denotes the strength of the next-nearest-neighbor hopping, J quantifies the interchain (rung) coupling, and Δ characterizes the onsite squeezing amplitude. **(b)** Spatial profiles of all eigenstates of the decoupled single chain under OBC, demonstrating the emergence of the $\mathbb{Z}_2$ skin effect in the decoupled limit. The parameters used are $J=0$, $t_1=2$, $t_2=1$, $\lambda=1$, and $\Delta=1/3$.

and B of the j-th unit cell in chain $s=1,2$, and L is the total number of unit cells. The parameters t_1 and t_2 denote the intracell and intercell hopping amplitudes along each leg, λ represents the next-nearest-neighbor hopping strength along each leg, and J quantifies the rung coupling between the two chains. The onsite squeezing amplitude Δ, induced via parametric driving, explicitly breaks particle-number conservation. Experimental realizations of such onsite squeezing have been reported in nanophotonic systems [111, 112], optomechanical platforms [113–115], and superconducting quantum circuits [116–119].

To analyze the impact of squeezing on the quasiparticle spectrum, we reformulate the Hamiltonian in Eq. (1) in momentum space within the Bogoliubov–de Gennes (BdG) framework. Introducing the Nambu spinor, $\hat{\Psi}_k=(\hat{a}_{1,k},\hat{b}_{1,k},\hat{a}_{2,k},\hat{b}_{2,k},\hat{a}^\dagger_{1,-k},\hat{b}^\dagger_{1,-k},\hat{a}^\dagger_{2,-k},\hat{b}^\dagger_{2,-k})^{\mathrm{T}}$, the Bloch Hamiltonian reads

$$\hat{H}_{\mathrm{B}}(k)=\frac{1}{2}\sum_k \hat{\Psi}^\dagger_k\,\mathcal{H}_{\mathrm{B}}(k)\,\hat{\Psi}_k+C, \tag{2}$$

where the BdG Hamiltonian takes the canonical block structure

$$\mathcal{H}_{\mathrm{B}}(k)=\begin{pmatrix}\mathcal{H}_0(k) & \Delta(k)\\ \Delta^*(-k) & \mathcal{H}_0^*(-k)\end{pmatrix}, \tag{3}$$

and the constant energy shift $C=-\mathrm{Tr}[\mathcal{H}_0(k)]/2$. The normal (single-particle) term, $\mathcal{H}_0(k)$ is explicitly given by

$$\begin{aligned}\mathcal{H}_0(k)=&(t_1+t_2\cos k)\tau_0\sigma_x+t_2\sin k\tau_0\sigma_y\\&+2\lambda\sin k\tau_0\sigma_z+J\tau_x\sigma_0,\end{aligned} \tag{4}$$

where the Pauli matrices σ_μ $(\mu=x,y,z)$ acts on the sublattices (A,B) degrees of freedom, τ_μ acts on the chain $(s=1,2)$ degrees of freedom, and σ_0 and τ_0 denote identity matrices. The pairing term $\Delta(k)=\Delta\tau_0\sigma_0$ encodes onsite bosonic squeezing.

Although $\mathcal{H}_{\mathrm{B}}(k)$ is Hermitian, the physical quasiparticle modes are governed by the non-Hermitian matrix arising from the canonical commutation relations $[\hat{\Psi}_k,\hat{\Psi}^\dagger_{k'}]=S_z\delta_{kk'}$. This intrinsic non-Hermiticity becomes evident in the Heisenberg equation of motion for the Nambu spinor,

$$\mathrm{i}\frac{\partial}{\partial_t}\hat{\Psi}_k=[\hat{\Psi}_k,\hat{H}_{\mathrm{B}}(k)]=\mathcal{M}_{\mathrm{B}}(k)\hat{\Psi}_k, \tag{5}$$

where the non-Hermitian dynamical matrix is defined as

$$\mathcal{M}_{\mathrm{B}}(k)=S_z\mathcal{H}_{\mathrm{B}}(k), \tag{6}$$

with $S_z=\nu_z\tau_0\sigma_0$, where ν_μ acts on particle–hole degrees of freedom. We note that if $\mathcal{H}_{\mathrm{B}}(k)$ is positive definite, all eigenvalues of $\mathcal{M}_{\mathrm{B}}(k)$ are real, yielding purely oscillatory dynamics coinciding with the Bogoliubov spectrum. If not, $\mathcal{M}_{\mathrm{B}}(k)$ can have complex eigenvalues, corresponding to exponentially growing or decaying modes, i.e., dynamical instabilities.

One can find that $\mathcal{M}_{\mathrm{B}}(k)$ satisfies several key symmetries: the pseudo-Hermiticity

$$\eta\mathcal{M}^\dagger_{\mathrm{B}}(k)\eta^{-1}=\mathcal{M}_{\mathrm{B}}(k),\quad \text{with } \eta=\tau_z\tau_0\sigma_0, \tag{7}$$

the particle-hole symmetry,

$$\mathcal{C}\mathcal{M}^*_{\mathrm{B}}(-k)\mathcal{C}^{-1}=-\mathcal{M}_{\mathrm{B}}(k),\quad \text{with } \mathcal{C}=\nu_x\tau_0\sigma_0, \tag{8}$$

the inversion symmetry

$$\mathcal{P}\mathcal{M}_{\mathrm{B}}(-k)\mathcal{P}^{-1}=\mathcal{M}_{\mathrm{B}}(k),\quad \text{with } \mathcal{P}=\nu_0\tau_0\sigma_x, \tag{9}$$

and mirror symmetry

$$\Theta\mathcal{M}_{\mathrm{B}}(k)\Theta^{-1}=\mathcal{M}_{\mathrm{B}}(k),\quad \text{with } \Theta=\nu_0\tau_x\sigma_0. \tag{10}$$

For the coupled bosonic chains, the symmetries of $\mathcal{M}_{\mathrm{B}}(k)$ [Eqs. (8)–(10)] ensure that its quasiparticle spectrum remains fourfold degenerate. Diagonalization of $\mathcal{M}_{\mathrm{B}}(k)$ yields two pairs of quasiparticle branches with squared energies

$$E^2_\pm(k)=\varepsilon(k)\pm\gamma(k), \tag{11}$$

where

$$\varepsilon(k)=J^2+t_1^2+t_2^2-\Delta^2+2\lambda^2+2t_1t_2\cos k-2\lambda^2\cos 2k, \tag{12}$$

$$\begin{aligned}\gamma(k)=2\big[&2\lambda^2(J+\Delta)(J-\Delta)(1-\cos 2k)\\&+J^2(t_1^2+t_2^2)+2t_1t_2J^2\cos k\big]^{1/2}.\end{aligned} \tag{13}$$

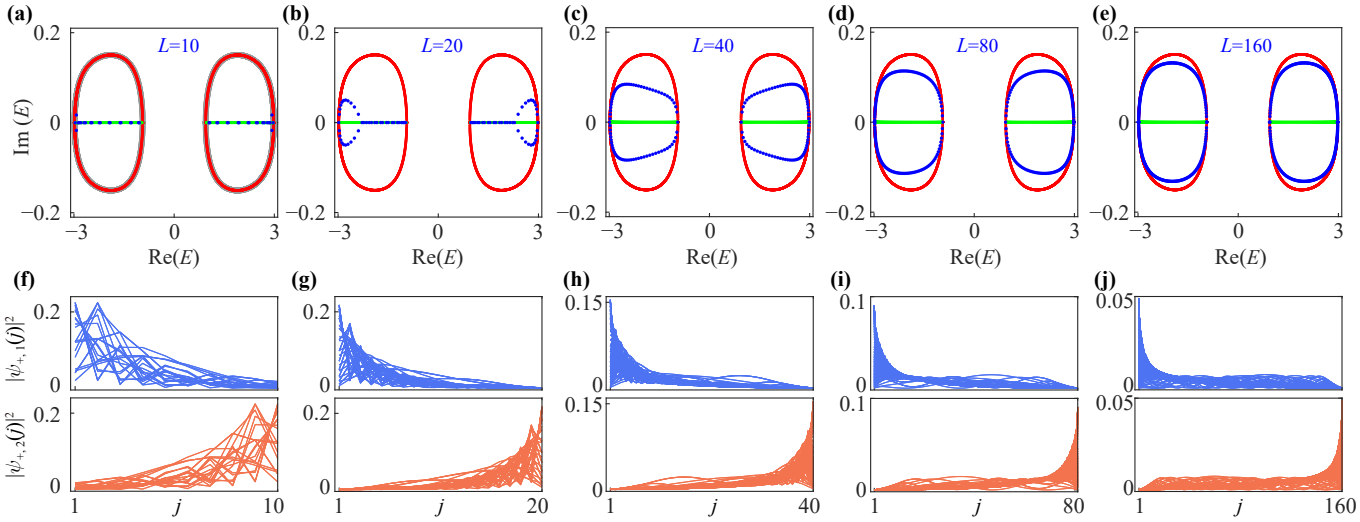

Fig. 2 **(a–e)** Complex eigenenergies of quasiparticle excitations obtained from $\mathcal{M}+$, the real-space representation of $\mathcal{M}_+(k)$, for different system sizes. Gray dots in (a) indicate the spectra under PBC, while red and blue dots correspond to the spectra in the infinite-size limit and for finite systems under OBC in the coupled-chain system, respectively. For comparison, green dots show the spectra in the infinite-size limit under OBC in the decoupled-chain limit. **(f–j)** Spatial distributions of all eigenstates of $\mathcal{M}_+$, showing the probability densities on chain 1, $|\psi+,1(j)|^2$ (top panels, blue), and on chain 2, $|\psi_{+,2}(j)|^2$ (bottom panels, orange). Parameters used are $J = 0.01$, $t_1 = 2$, $t_2 = 1$, $\lambda = 1/2$, and $\Delta = 1/3$.

To make this degeneracy structure explicit, we employ the unitary transformation

$$U_k = \frac{1}{\sqrt{2}} \begin{pmatrix} \mathrm{i}\tau_z\sigma_z & \tau_0\sigma_0 \\ -\mathrm{i}\tau_z\sigma_z & \tau_0\sigma_0 \end{pmatrix}, \tag{14}$$

which block-diagonalizes $\mathcal{M}_{\mathrm{B}}(k)$ into two independent blocks,

$$U_k\mathcal{M}_{\mathrm{B}}(k)U_k^\dagger = \begin{pmatrix} \mathcal{M}_+(k) & 0 \\ 0 & \mathcal{M}_-(k) \end{pmatrix}, \tag{15}$$

with

$$\begin{aligned}\mathcal{M}_\pm(k) = & -(t_1 + t_2\cos k)\tau_0\sigma_x - t_2\sin k\tau_0\sigma_y \\ & + 2\lambda\sin k\tau_0\sigma_z - J\tau_x\sigma_0 \pm \mathrm{i}\Delta\tau_z\sigma_z.\end{aligned} \tag{16}$$

Each block $\mathcal{M}_\pm(k)$ possesses the identical eigenvalue set, $\{\pm E_+(k), \pm E_-(k)\}$. Consequently, each block retains an internal twofold degeneracy, analogous to that of an isolated single chain. We emphasize that this transformation acts solely at the level of the dynamical matrix. It does not redefine the quasiparticle operators and therefore leaves the symplectic structure of the bosonic BdG problem intact, preserving the canonical commutation relations.

3 Quantum squeezing-induced critical skin effect emerging from $\mathbb{Z}_2$ skin modes in the decoupled limit

Previous studies of the critical cNHSE have largely focused on systems composed of coupled distinct non-Hermitian chains with different NHSE decay lengths [74–79], where each chain hosts skin-mode localization at opposite boundaries. In contrast, the Hermitian bosonic ladder considered here consists of two identical chains. In the decoupled limit ($J = 0$), each chain exhibits a twofold quasiparticle degeneracy protected jointly by particle–hole and inversion symmetries [105]. Under open boundary conditions, the eigenstates of each isolated chain become localized at opposite ends of the system, providing a direct manifestation of the Hermitian $\mathbb{Z}_2$ skin effect, as shown in Fig. 1(b). Building on this setting, we explore the possibility of realizing a cNHSE in Hermitian bosonic quadratic lattices, where each individual chain already supports a $\mathbb{Z}_2$ skin effect in the decoupled limit, fundamentally distinct from previously studied cNHSE scenarios.

Due to the degeneracy of $\mathcal{M}_{\mathrm{B}}(k)$, any of its physical eigenstates can be expressed as a linear combination of states from the decoupled components $\mathcal{M}_\pm(k)$. Without loss of generality, we work with $\mathcal{M}_+$ [the real-space representation of $\mathcal{M}_+(k)$] for the numerical simulations.

To demonstrate the emergence of the critical skin effect in a Hermitian bosonic quadratic Hamiltonian with $\mathbb{Z}_2$ skin effect, we analyze the complex quasiparticle eigenenergies obtained from $\mathcal{M}_+$ for various system sizes, as shown in Figs. 2(a)–(e). In Fig. 2(a), the OBC spectrum in the thermodynamic limit, computed using non-Bloch band theory (red dots), coincides with the PBC spectrum (gray dots) of the coupled-chain system. In contrast, for two decoupled chains in the infinite-size limit, the OBC spectrum remains entirely real (green

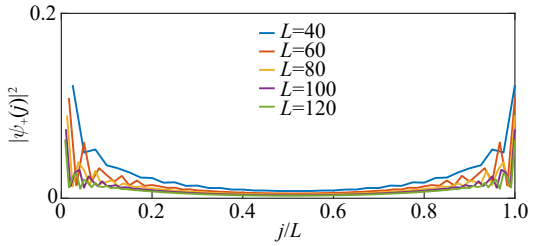

Fig. 3 Spatial distribution of the eigenstates $|\psi_+(j)|^2$ of $\mathcal{M}_+$ corresponding to the eigenvalue with the largest imaginary part, $\mathrm{Max}[\mathrm{Im}(E_{\mathrm{OBC}})]$, and negative real part, for various system sizes. The parameters used are $J = 0.01$, $t_1 = 2$, $t_2 = 1$, $\lambda = 1/2$, and $\Delta = 1/3$.

dots), and is clearly distinct from that of the coupled case. This discontinuous change of the OBC spectrum across the critical point $J = 0$ in the thermodynamic limit signals the emergence of the critical skin effect, where the simple $\mathbb{Z}_2$-type pairing structure of the decoupled chains no longer applies.

For finite systems, this discontinuity is smoothed into a continuous crossover. At small sizes, such as $L = 10$, the OBC spectrum remains nearly real and closely coincides with the decoupled-chain spectrum, indicating that the effect of interchain coupling is negligible [see the overlap of blue and green dots in Fig. 2(a)]. As the system size increases, however, the OBC spectrum gradually acquires a finite imaginary part and spreads into the complex plane. In the thermodynamic limit, it converges toward the Bloch spectrum, as seen from the approach of the blue dots to the red dots in Figs. 2(b)–(e). This spectral evolution is accompanied by a corresponding change in the wave functions: initially localized states become increasingly extended as the spectrum approaches the Bloch limit [see spatial distribution of all eigenstates of $\mathcal{M}_+(k)$ in Figs. 2(f)–(j)].

Another hallmark of this critical behavior is scale-free localization, manifested by a localization length that increases with system size. Figure 3 illustrates the spatial distribution of the eigenstates $|\psi_+(j)|^2$ of $\mathcal{M}_+$ corresponding to the OBC eigenvalue with the largest imaginary part of $\mathrm{Max}[\mathrm{Im}(E_{\mathrm{OBC}})]$ and with negative real part, for system sizes $L = 40, 60, 80, 100, 120$. The horizontal axis is normalized by L, demonstrating the scale-free character of the localization.

On the other hand, the size-dependent evolution of the imaginary part of the quasiparticle spectrum has direct consequences for the system's dynamical behavior. For small systems, the purely real spectrum indicates dynamical stability [see Fig. 2(a)]. Beyond a critical system size, however, the emergence of a finite imaginary component leads to dynamical instability [see Figs. 2(b)–(e)]. This behavior is qualitatively different from conventional non-Hermitian systems with explicit gain and loss, where instability is typically parameter-driven. In contrast, here both the onset and the strength of instability can be controlled by the system size, reflecting a boundary-sensitive mechanism enabled by the critical non-Hermitian skin effect. We refer to this behavior as size-dependent dynamical instability, a phenomenon that is absent in Hermitian single-particle systems as well as in non-Hermitian systems without gain. This dynamical instability gives rise to system-size-dependent quantum signal amplification, where the amplification factor, quantified by the maximum imaginary part of the spectrum, is directly controlled by the lattice dimensions.

4 Size-dependent skin transition

The eigenenergy spectrum of $\mathcal{M}_+(k)$ is constrained by particle–hole and inversion symmetries, resulting in a twofold degeneracy associated with opposite spectral winding across the Brillouin zone. We show that introducing a staggered onsite squeezing perturbation breaks inversion symmetry and lifts this degeneracy. Moreover, it induces a size-dependent skin transition and enhances boundary localization.

Specifically, we consider a staggered onsite squeezing perturbation that modifies the original pairing matrix as

$$\Delta'(k) = \Delta(k) + V\tau_0\sigma_z, \tag{17}$$

which preserves the Hermiticity of the bosonic ladder system. While the perturbation breaks the inversion symmetry of $\mathcal{M}_{\mathrm{B}}(k)$, the mirror symmetry remains intact. Applying the same unitary transformation as in Eq. (14) to separate the degenerate subspaces, the reduced matrices are modified as

$$\mathcal{M}'_{\pm}(k) = \mathcal{M}_{\pm}(k) \pm \mathrm{i}V\tau_z\sigma_0, \tag{18}$$

where the term $\mathrm{i}V\tau_z\sigma_0$ acts as an effective staggered loss.

Figures 4(a)–(e) present the eigenenergies of quasiparticle excitations computed from $\mathcal{M}'_+$ for different system sizes. Under PBC, the staggered onsite squeezing perturbation lifts the degeneracy and splits the spectrum into two bands with opposite spectral winding as k varies from $-\pi$ to π, as indicated by the black solid and dashed lines with arrows in Fig. 4(a). In the thermodynamic limit, the OBC spectrum lies between these two winding branches, as shown by the red lines in Fig. 4(a). For comparison, the OBC spectrum in the infinite-size limit for the decoupled chain is also displayed (green lines). Notably, the discontinuous jump of the OBC spectrum across the critical point persists even in the presence of the staggered onsite squeezing, indicating that the critical skin effect remains intact.

In finite systems, the behavior is qualitatively different. For small system sizes, for example $L = 10$, the OBC spectrum (blue dots) closely follows that of the decoupled limit (green lines), as shown in Fig. 4(a), indi-

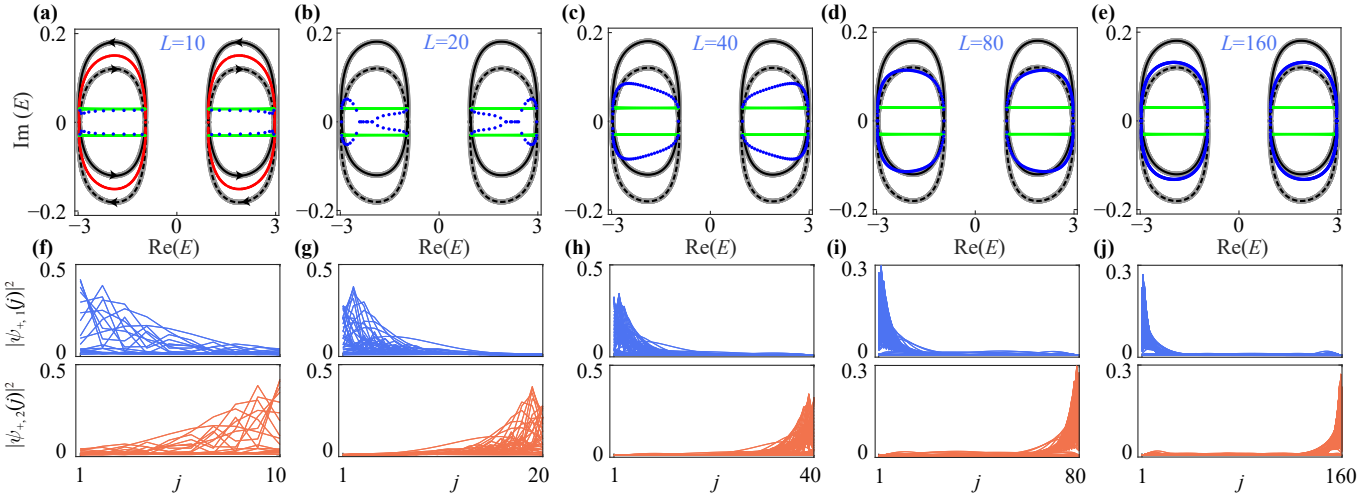

Fig. 4 **(a–e)** Complex eigenenergies of quasiparticle excitations obtained from $\mathcal{M}'_+$, the real-space representation of $\mathcal{M}'_+(k)$, for different system sizes. The red lines in (a) indicate the spectrum in the infinite-size limit under OBC. Black solid and dashed lines with arrows denote the spectra under PBC for the coupled-chain system, where the arrows indicate the spectral winding as k traverses the Brillouin zone. Blue dots correspond to the spectra of finite coupled chains under OBC. For comparison, the green lines show the spectra in the infinite-size limit under OBC in the decoupled-chain limit. **(f–j)** Spatial distributions of all eigenstates of $\mathcal{M}'_+$, showing the probability densities on chain 1, $|\psi_{+,1}(j)|^2$ (top panels, blue), and on chain 2, $|\psi_{+,2}(j)|^2$ (bottom panels, orange). Parameters used are $J = 0.01$, $V = 0.03$, $t_1 = 2$, $t_2 = 1$, $\lambda = 1/2$, and $\Delta = 1/3$.

cating that the staggered onsite squeezing perturbation has a negligible effect at small sizes. As the system size increases, the spectrum progressively spreads into the complex plane, crossing the loop formed by the PBC spectrum and undergoing a sequence of phase transitions characterized by changes in the point-gap topology [blue dots in Figs. 4(b)–(e)]. This evolution reflects the gradual emergence of a size-dependent skin effect, which we refer to as the size-dependent skin transition.

To characterize this transition, we introduce the spectral winding number [38, 52, 56], defined as

$$\mathcal{W}(E_0) = \int_{\mathrm{BZ}} \frac{\mathrm{d}k}{2\pi \mathrm{i}} \partial_k \ln \det[\mathcal{M}'_+(k) - E_0], \tag{19}$$

where E_0 is a reference point located inside a point-gap loop. The integer $\mathcal{W}(E_0)$ counts the number of times the complex spectrum of $\mathcal{M}'_+(k)$ encircles E_0.

Applying Eq. (19) to the PBC spectrum at $L = 80$, as shown in Figs. 5(a, b), we identify three distinct regions: $\mathcal{W} = -1$ for the clockwise loop (red), $\mathcal{W} = 1$ for the counterclockwise loop (green), and $\mathcal{W} = 0$ for the region enclosed by both loops (blue). For system sizes $L < 80$, the OBC eigenenergies initially reside within the $\mathcal{W} = 0$ region and gradually evolve into a closed loop in the complex plane. As L increases, this loop expands, and once $L > 80$, it extends into both the $\mathcal{W} = 1$ and $\mathcal{W} = -1$ regions. This behavior indicates that the coupled ladder undergoes a size-dependent skin transition, reflecting the gradual emergence of a size-dependent skin effect.

As the complex quasiparticle eigenenergies undergo a

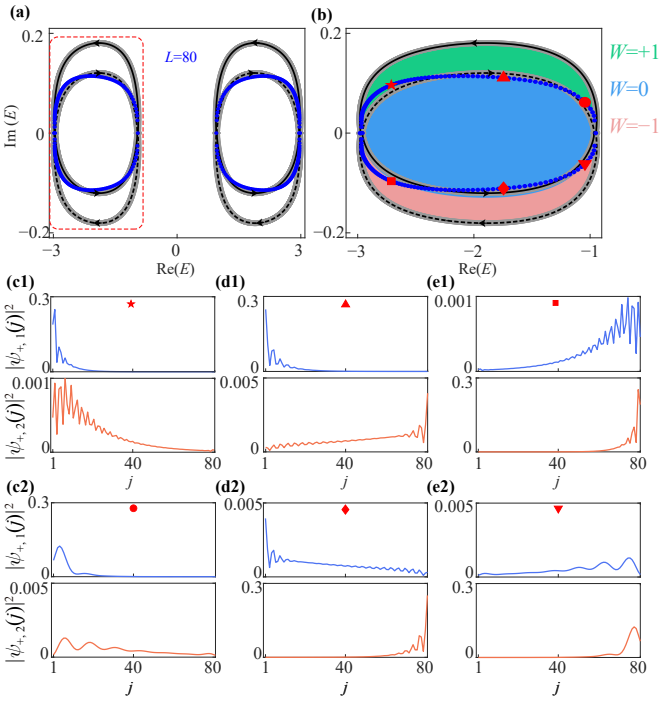

Fig. 5 **(a)** Complex eigenenergies of quasiparticle excitations computed from $\mathcal{M}'_+$ at $L = 80$. **(b)** Enlarged view of the red dotted region in (a). The red, blue, and green shaded areas denote point-gap regions with winding numbers $\mathcal{W} = -1$, 0, and 1, respectively. **(c1–e2)** Spatial distributions of representative eigenstates indicated by the red markers in (b). For each case, the probability density on chain 1, $|\psi_{+,1}(j)|^2$ (top, blue), and on chain 2, $|\psi_{+,2}(j)|^2$ (bottom, orange), are shown for (c1, c2) $\mathcal{W} = 1$, (d1, d2) $\mathcal{W} = 0$, and (e1, e2) $\mathcal{W} = -1$.

size-dependent skin transition under OBC, the corresponding eigenstates simultaneously exhibit a change in their skin localization properties. To characterize this transition, we compute the spatial distributions of representative eigenstates on chain 1, $|\psi_{+,1}(j)|^2$, and on chain 2, $|\psi_{+,2}(j)|^2$ [indicated by red markers in Fig. 5(b)]. When the OBC complex energy lies in the $\mathcal{W}=1$ ($\mathcal{W}=-1$) region, the eigenstates exhibit a unipolar non-Hermitian skin effect, being localized at the left (right) boundary on both chains, as shown in Figs. 5(c1, c2) and (e1, e2). In contrast, when the complex eigenenergy under OBC lies in the $\mathcal{W}=0$ region, the eigenstates display a bipolar non-Hermitian skin effect, with simultaneous localization at opposite boundaries of the two chains, as shown in Figs. 5(d1,d2).

Moreover, the staggered onsite squeezing perturbation substantially enhances boundary localization of the eigenstates in the coupled chains. In the absence of this perturbation, the OBC spectrum progressively converges to the Bloch spectrum in the thermodynamic limit, and the eigenstates become increasingly extended and Bloch-like as the system size increases, as shown in Figs. 3(f)–(j). By contrast, upon introducing the perturbation, the OBC spectrum remains confined to the $\mathcal{W}=1$ and $\mathcal{W}=-1$ sectors even in the thermodynamic limit. This behavior indicates that the eigenstates are dominated by the skin effect and consequently remain robustly localized at opposite boundaries of the two chains, as shown in Figs. 4(f)–(j).

The enhancement of boundary localization can be quantitatively characterized by evaluating the maximum and mean inverse participation ratio (IPR) over all eigenstates of $\mathcal{M}_+$ and $\mathcal{M}'_+$, and qualitatively captured using generalized Brillouin zone (GBZ).

The IPR of the i-th normalized eigenstate $\psi_+(i,j)$ is defined as

$$\mathrm{IPR}(i)=\sum_{j}^{L}|\psi_+(i,j)|^4. \tag{20}$$

The GBZs of the 4×4 non-Bloch matrices $\mathcal{M}_+$ and $\mathcal{M}'_+$ can be derived by solving the characteristic equations [37]

$$\det[\mathcal{M}_+(\beta)-E]=0, \tag{21}$$

and

$$\det[\mathcal{M}'_+(\beta)-E]=0. \tag{22}$$

These equations yield four solutions β_1, β_2, β_3, and β_4, which are ordered according to their moduli as $|\beta_1|\le|\beta_2|\le|\beta_3|\le|\beta_4|$.

In the thermodynamic limit $L\to\infty$, the GBZ is determined by the condition

$$|\beta_2|=|\beta_3|. \tag{23}$$

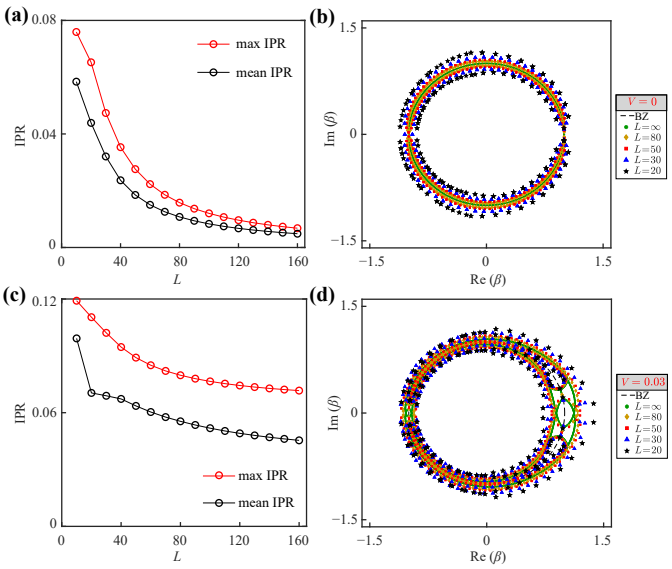

Fig. 6 The maximum (red dotted lines) and mean (black dotted lines) IPR, evaluated over all eigenstates, are plotted as functions of the system size L for **(a)** $V=0$ and **(c)** $V=0.03$. Panels **(b)** and **(d)** show the GBZ of the coupled system at finite sizes $L=20$ (black), 30 (blue), 50 (red), and 80 (yellow), as well as in the thermodynamic limit $L\to\infty$ (green), for (b) $V=0$ and (d) $V=0.03$, respectively. For finite L, the GBZ is determined from the characteristic equation in Eqs. (21) and (22) using numerically obtained OBC eigenenergies E_{OBC}. In the thermodynamic limit, it is obtained from the condition $|\beta_2|=|\beta_3|$. Parameters used are $J=0.01$, $t_1=2$, $t_2=1$, $\lambda=1/2$, and $\Delta=1/3$.

By contrast, for finite system sizes, the GBZ is obtained by numerically solving the characteristic equations in Eqs. (21) and (22) using the numerically computed OBC spectrum E_{OBC}. In this procedure, the Bloch wavevector is analytically continued into the complex plane as $k\to\tilde{k}=k+\mathrm{i}r$ $(r\in\mathbb{R})$, with $\beta=\mathrm{e}^{\mathrm{i}\tilde{k}}$.

Figures 6(a) and (c) show that for $V=0$, both the maximum and mean IPR gradually decrease toward zero as L increases, indicating that the eigenstates become increasingly extended and Bloch-like. In contrast, for $V=0.03$, the IPR remains finite even for large system sizes, demonstrating that the staggered onsite squeezing perturbation preserves and enhances boundary localization via the skin effect. Correspondingly, as shown in Figs. 6(b) and (d), the generalized Brillouin zone (GBZ) gradually approaches the unit circle for $V=0$, whereas for $V=0.03$, the GBZ deviates significantly from the unit circle, reflecting the persistent boundary-localized nature of the eigenstates.

5 Conclusion

We have shown that Hermitian bosonic lattices with onsite squeezing can realize a critical NHSE driven

purely by the intrinsic non-Hermiticity of the BdG dynamics. The spectrum exhibits a discontinuous jump in the thermodynamic limit and scale-free localization with size-dependent instability in finite systems. Breaking inversion symmetry via staggered squeezing lifts degeneracies and induces a size-dependent skin transition with robust boundary localization. These results extend critical NHSE physics to coherent bosonic platforms and provide new opportunities for controlling non-Bloch dynamics without engineered dissipation. We emphasize that the $\mathbb{Z}_2$ skin effect discussed in this work characterizes the decoupled chains, while the emergent critical behavior in the coupled system is not constrained by a $\mathbb{Z}_2$ classification.

Declarations The authors declare that they have no competing interests and there are no conflicts.

Acknowledgements T.L. acknowledges the support from Guangdong Provincial Quantum Science Strategic Initiative (Grant No. GDZX2505004) and the Introduced Innovative Team Project of Guangdong Pearl River Talents Program (Grant No. 2021ZT09Z109).

References

1. Y. Ashida, Z. Gong, and M. Ueda, Non-Hermitian physics, *Adv. Phys.* 69(3), 249 (2020)
2. K. Kawabata, K. Shiozaki, M. Ueda, and M. Sato, Symmetry and topology in non-Hermitian physics, *Phys. Rev. X* 9(4), 041015 (2019)
3. Z. Gong, Y. Ashida, K. Kawabata, K. Takasan, S. Higashikawa, and M. Ueda, Topological phases of non-Hermitian systems, *Phys. Rev. X* 8(3), 031079 (2018)
4. E. J. Bergholtz, J. C. Budich, and F. K. Kunst, Exceptional topology of non-Hermitian systems, *Rev. Mod. Phys.* 93(1), 015005 (2021)
5. T. Micallo, C. Lehmann, and J. C. Budich, Correlation-induced sensitivity and non-Hermitian skin effect of quasiparticles, *Phys. Rev. Res.* 5(4), 043105 (2023)
6. C. Leefmans, A. Dutt, J. Williams, L. Yuan, M. Parto, F. Nori, S. Fan, and A. Marandi, Topological dissipation in a time-multiplexed photonic resonator network, *Nat. Phys.* 18(4), 442 (2022)
7. M. Reisenbauer, H. Rudolph, L. Egyed, K. Hornberger, A. V. Zasedatelev, M. Abuzarli, B. A. Stickler, and U. Delić, Non-Hermitian dynamics and non-reciprocity of optically coupled nanoparticles, *Nat. Phys.* 20(10), 1629 (2024)
8. K. Ochkan, R. Chaturvedi, V. Könye, L. Veyrat, R. Giraud, D. Mailly, A. Cavanna, U. Gennser, E. M. Hankiewicz, B. Büchner, J. van den Brink, J. Dufouleur, and I. C. Fulga, Non-Hermitian topology in a multiterminal quantum hall device, *Nat. Phys.* 20(3), 395 (2024)
9. Y. M. Hu, H. Y. Wang, Z. Wang, and F. Song, Geometric origin of non-Bloch PT symmetry breaking, *Phys. Rev. Lett.* 132(5), 050402 (2024)
10. S. Longhi, Erratic non-Hermitian skin localization, *Phys. Rev. Lett.* 134(19), 196302 (2025)
11. B. Li, C. Chen, and Z. Wang, Universal non-Hermitian transport in disordered systems, *Phys. Rev. Lett.* 135(3), 033802 (2025)
12. S. X. Wang and Z. Yan, Enhanced sensitivity in non-Hermitian systems at infernal points, *Phys. Rev. Res.* 7(2), L022037 (2025)
13. J. Gliozzi, G. De Tomasi, and T. L. Hughes, Many body non-Hermitian skin effect for multipoles, *Phys. Rev. Lett.* 133(13), 136503 (2024)
14. T. Yoshida, S. B. Zhang, T. Neupert, and N. Kawakami, Non-Hermitian Mott skin effect, *Phys. Rev. Lett.* 133(7), 076502 (2024)
15. A. Yang, Z. Fang, K. Zhang, and C. Fang, Tailoring bound state geometry in high-dimensional non-Hermitian systems, *Commun. Phys.* 8(1), 124 (2025)
16. P. Molignini, O. Arandes, and E. J. Bergholtz, Anomalous skin effects in disordered systems with a single non-Hermitian impurity, *Phys. Rev. Res.* 5(3), 033058 (2023)
17. H. Jiang, and C. H. Lee, Dimensional transmutation from non-Hermiticity, *Phys. Rev. Lett.* 131(7), 076401 (2023)
18. X. Cheng, H. Jiang, J. Chen, L. Zhang, Y. S. Ang, and C. H. Lee, Non-Hermitian effective PT-symmetry restoration from structural disorder, *Front. Phys.* 21, 035201 (2026)
19. C. A. Li, B. Trauzettel, T. Neupert, and S. B. Zhang, Enhancement of second-order non-Hermitian skin effect by magnetic fields, *Phys. Rev. Lett.* 131(11), 116601 (2023)
20. Z. Gong, M. Bello, D. Malz, and F. K. Kunst, Anomalous behaviors of quantum emitters in non-Hermitian baths, *Phys. Rev. Lett.* 129(22), 223601 (2022)
21. Z. F. Cai, Y. C. Wang, Y. R. Zhang, T. Liu, and F. Nori, Versatile control of nonlinear topological states in non-Hermitian systems, *Commun. Phys.* 8(1), 360 (2025)
22. L. H. Mo, Z. Xiao, R. Moessner, and H. Zhao, Non-Hermitian delocalization in one dimension via emergent compactness, *Phys. Rev. B* 111(23), 235412 (2025)
23. Y. Y. Zou, Y. Zhou, L. M. Chen, and P. Ye, Detecting bulk and edge exceptional points in non-Hermitian systems through generalized petermann factors, *Front. Phys. (Beijing)* 19(2), 023201 (2024)
24. D. C. Ohnmacht, V. Wilhelm, H. Weisbrich, and W. Belzig, Non-Hermitian topology in multiterminal superconducting junctions, *Phys. Rev. Lett.* 134(15), 156601 (2025)
25. J. Shi and A. N. Poddubny, Chiral dissociation of bound photon pairs for a non-Hermitian skin effect, *Phys. Rev. Lett.* 134(23), 233602 (2025)
26. A. Hashemi, E. L. Pereira, H. Li, J. L. Lado, and A. Blanco-Redondo, Observation of non-Hermitian topology from optical loss modulation, *Nat. Mater.* 24(9), 1393 (2025)
27. K. Sun and H. Hu, Lyapunov formulation of band theory for disordered non-Hermitian systems, arXiv: 2507.09447 (2025)
28. D. Nakamura, K. Shiozaki, K. Shimomura, M. Sato, and K. Kawabata, Non-Hermitian origin of detachable

boundary states in topological insulators, *Phys. Rev. Lett.* 135(9), 096601 (2025)
29. B. B. Wang, Z. Cheng, H. Y. Zou, Y. Ge, K. Q. Zhao, Q. R. Si, S. Q. Yuan, H. X. Sun, H. Xue, and B. Zhang, Observation of disorder-induced boundary localization, *Proc. Natl. Acad. Sci. USA* 122(19), e2422154122 (2025)
30. S. M. Hosseiny, H. R. Jahromi, B. Farajollahi, and M. Amniat-Talab, Technique for studying the coalescence of eigenstates and eigenvalues in non-Hermitian systems, *Front. Phys. (Beijing)* 20(1), 014201 (2025)
31. J. P. Esparza, and V. Juričić, Exceptional magic angles in non-Hermitian twisted bilayer graphene, *Phys. Rev. Lett.* 134(22), 226602 (2025)
32. T. R. Liu, T. Liu, and M. Xiao, Anomalous non-Hermitian skin effect of chiral boundary states, *Phys. Rev. B* 112(8), L081112 (2025)
33. N. Zeng, T. Liu, K. Xia, Y. R. Zhang, and F. Nori, Non-Hermitian sensing from the perspective of post-selected measurements, *Phys. Rev. Res.* 7(4), 043219 (2025)
34. Z. F. Cai, Y. Li, Y. R. Zhang, X. Wei, Z. Yang, T. Liu, and F. Nori, Arbitrary control of non-Hermitian skin modes via disorder and an electric field, arXiv: 2511.16393 (2025)
35. L. Kong, M. H. Eldegail, and C. Xu, Extension of coherent perfect absorption-lasing effect and supercollimation effect in an airborne phononic crystal with space-coiling structure, *Front. Phys. (Beijing)* 21(2), 015201 (2026)
36. S. Yao and Z. Wang, Edge states and topological invariants of non-Hermitian systems, *Phys. Rev. Lett.* 121(8), 086803 (2018)
37. K. Yokomizo, and S. Murakami, Non-Bloch band theory of non-Hermitian systems, *Phys. Rev. Lett.* 123(6), 066404 (2019)
38. K. Zhang, Z. Yang, and C. Fang, Correspondence between winding numbers and skin modes in non-Hermitian systems, *Phys. Rev. Lett.* 125(12), 126402 (2020)
39. T. Liu, Y. R. Zhang, Q. Ai, Z. Gong, K. Kawabata, M. Ueda, and F. Nori, Second-order topological phases in non-Hermitian systems, *Phys. Rev. Lett.* 122(7), 076801 (2019)
40. F. K. Kunst, E. Edvardsson, J. C. Budich, and E. J. Bergholtz, Biorthogonal bulk–boundary correspondence in non-Hermitian systems, *Phys. Rev. Lett.* 121(2), 026808 (2018)
41. W. Z. Ling, Z. F. Cai, and T. Liu, Interaction-induced second-order skin effect, *Phys. Rev. B* 111(20), 205418 (2025)
42. Y. Li, Z. F. Cai, T. Liu, and F. Nori, Dissipation and interaction-controlled non-Hermitian skin effects, *Phys. Rev. B* 113(3), 035444 (2026)
43. Z. Gong, Y. Ashida, K. Kawabata, K. Takasan, S. Higashikawa, and M. Ueda, Topological phases of non-Hermitian systems, *Phys. Rev. X* 8(3), 031079 (2018)
44. S. Yao, F. Song, and Z. Wang, Non-Hermitian Chern bands, *Phys. Rev. Lett.* 121(13), 136802 (2018)
45. F. Song, S. Yao, and Z. Wang, Non-Hermitian skin effect and chiral damping in open quantum systems, *Phys. Rev. Lett.* 123(17), 170401 (2019)
46. J. Y. Lee, J. Ahn, H. Zhou, and A. Vishwanath, Topological correspondence between Hermitian and non-Hermitian systems: Anomalous dynamics, *Phys. Rev. Lett.* 123(20), 206404 (2019)
47. K. Kawabata, T. Bessho, and M. Sato, Classification of exceptional points and non-Hermitian topological semimetals, *Phys. Rev. Lett.* 123(6), 066405 (2019)
48. J. Zhang, B. Peng, Ş. K. Özdemir, K. Pichler, D. O. Krimer, G. Zhao, F. Nori, Y. Liu, S. Rotter, and L. Yang, A phonon laser operating at an exceptional point, *Nat. Photonics* 12(8), 479 (2018)
49. Z. Y. Ge, Y. R. Zhang, T. Liu, S. W. Li, H. Fan, and F. Nori, Topological band theory for non-Hermitian systems from the Dirac equation, *Phys. Rev. B* 100(5), 054105 (2019)
50. F. Minganti, A. Miranowicz, R. W. Chhajlany, and F. Nori, Quantum exceptional points of non-Hermitian Hamiltonians and Liouvillians: The effects of quantum jumps, *Phys. Rev. A* 100(6), 062131 (2019)
51. H. Zhao, X. Qiao, T. Wu, B. Midya, S. Longhi, and L. Feng, Non-Hermitian topological light steering, *Science* 365(6458), 1163 (2019)
52. D. S. Borgnia, A. J. Kruchkov, and R. J. Slager, Non-Hermitian boundary modes and topology, *Phys. Rev. Lett.* 124(5), 056802 (2020)
53. V. M. Martinez Alvarez, J. E. Barrios Vargas, and L. E. F. Foa Torres, Non-Hermitian robust edge states in one dimension: Anomalous localization and eigenspace condensation at exceptional points, *Phys. Rev. B* 97(12), 121401 (2018)
54. I. I. Arkhipov, A. Miranowicz, F. Minganti, and F. Nori, Liouvillian exceptional points of any order in dissipative linear bosonic systems: Coherence functions and switching between PT and anti-PT symmetries, *Phys. Rev. A* 102(3), 033715 (2020)
55. T. Zheng, W. Lv, Y. Zhou, C. Xu, and M. H. Lu, Characterizing non-Hermitian topological monomodes via fractional mode charges in acoustic systems, *Front. Phys. (Beijing)* 20(1), 014202 (2025)
56. N. Okuma, K. Kawabata, K. Shiozaki, and M. Sato, Topological origin of non-Hermitian skin effects, *Phys. Rev. Lett.* 124(8), 086801 (2020)
57. T. Liu, J. J. He, Z. Yang, and F. Nori, Higher-order Weyl-exceptional-ring semimetals, *Phys. Rev. Lett.* 127(19), 196801 (2021)
58. Y. Xiao, H. L. Zhang, R. H. Zheng, J. Song, Y. H. Chen, Y. H. Kang, and Y. Xia, Parity detection based on non-Hermitian spectral phase transition, *Front. Phys. (Beijing)* 21(11), 115201 (2026)
59. Y. Li, C. Liang, C. Wang, C. Lu, and Y. C. Liu, Gain-loss-induced hybrid skin-topological effect, *Phys. Rev. Lett.* 128(22), 223903 (2022)
60. K. Li and Y. Xu, Non-Hermitian absorption spectroscopy, *Phys. Rev. Lett.* 129(9), 093001 (2022)
61. N. Zeng, T. Liu, K. Xia, Y. R. Zhang, and F. Nori, Non-Hermitian sensing from the perspective of postselected measurements, *Phys. Rev. Res.* 7(4), 043219 (2025)
62. Z. F. Cai, X. Wang, Z. X. Liang, T. Liu, and F. Nori, Chiral-extended photon-emitter dressed states in non-

Hermitian topological baths, *Phys. Rev. A* 111(6), L061701 (2025)
63. K. Zhang, C. Fang, and Z. Yang, Dynamical degeneracy splitting and directional invisibility in non-Hermitian systems, *Phys. Rev. Lett.* 131(3), 036402 (2023)
64. H. Wang, J. Liu, T. Liu, and W. B. Ju, Observation of impurity-induced scale-free localization in a disordered non-Hermitian electrical circuit, *Front. Phys. (Beijing)* 20(1), 014203 (2025)
65. J. R. Li, S. F. Zhang, C. H. Zhao, K. Du, L. L. Zhang, and W. J. Gong, Multiple competition between non-Hermitian skin effect and localization in a Su–Schrieffer–Heeger chain with unidirectional anderson disorder, *Front. Phys. (Beijing)* 21(9), 095201 (2026)
66. X. Li, J. Liu, and T. Liu, Localization-delocalization transitions in non-Hermitian Aharonov–Bohm cages, *Front. Phys. (Beijing)* 19(3), 33211 (2024)
67. W. W. Jin, J. Liu, X. Wang, Y. R. Zhang, X. Huang, X. Wei, W. Ju, Z. Yang, T. Liu, and F. Nori, Anderson delocalization in strongly coupled disordered non-Hermitian chains, *Phys. Rev. Lett.* 135(7), 076602 (2025)
68. M. Parto, C. Leefmans, J. Williams, F. Nori, and A. Marandi, Non-Abelian effects in dissipative photonic topological lattices, *Nat. Commun.* 14(1), 1440 (2023)
69. H. Y. Wang, F. Song, and Z. Wang, Amoeba formulation of non-Bloch band theory in arbitrary dimensions, *Phys. Rev. X* 14(2), 021011 (2024)
70. C. X. Guo, L. Su, Y. Wang, L. Li, J. Wang, X. Ruan, Y. Du, D. Zheng, S. Chen, and H. Hu, Scale-tailored localization and its observation in non-Hermitian electrical circuits, *Nat. Commun.* 15(1), 9120 (2024)
71. H. Q. Liang, Z. Ou, L. Li, and G. F. Xu, Intrinsic perturbation induced anomalous higher-order boundary states in non-Hermitian systems, *Phys. Rev. B* 111(24), L241112 (2025)
72. X. Wu, Y. Huang, H. Zhang, L. Wan, Y. Li, Y. Yang, H. Chen, and Z. Guo, Synthetic high-order non-Hermitian bound state in the continuum for enhanced wireless power transfer, *Front. Phys. (Beijing)* 21(4), 045202 (2026)
73. Y. Xiong, Z. Y. Xing, and H. Hu, Non-Hermitian skin effect in arbitrary dimensions: Non-Bloch band theory and classification, arXiv: 2407.01296 (2024)
74. L. Li, C. H. Lee, S. Mu, and J. Gong, Critical non-Hermitian skin effect, *Nat. Commun.* 11(1), 5491 (2020)
75. B. Li, H. R. Wang, F. Song, and Z. Wang, Scale-free localization and PT symmetry breaking from local nonHermiticity, *Phys. Rev. B* 108(16), L161409 (2023)
76. Z. F. Cai, T. Liu, and Z. Yang, Non-Hermitian skin effect in periodically driven dissipative ultracold atoms, *Phys. Rev. A* 109(6), 063329 (2024)
77. K. Yokomizo and S. Murakami, Scaling rule for the critical non-Hermitian skin effect, *Phys. Rev. B* 104(16), 165117 (2021)
78. S. M. Rafi-Ul-Islam, Z. B. Siu, H. Sahin, C. H. Lee, and M. B. A. Jalil, Critical hybridization of skin modes in coupled non-Hermitian chains, *Phys. Rev. Res.* 4(1), 013243 (2022)
79. F. Qin, Y. Ma, R. Shen, and C. H. Lee, Universal competitive spectral scaling from the critical non-Hermitian skin effect, *Phys. Rev. B* 107(15), 155430 (2023)
80. S. M. Rafi-Ul-Islam, Z. B. Siu, M. S. H. Razo, and M. B. A. Jalil, Critical non-Hermitian skin effect in a cross-coupled Hermitian chain, *Phys. Rev. B* 111(11), 115415 (2025)
81. M. Sanahal, S. Panda, and S. Nandy, Gauge field induced skin effect in spinful non-Hermitian systems, *Phys. Rev. B* 112(12), 125149 (2025)
82. L. Li, W. X. Teo, S. Mu, and J. Gong, Direction reversal of non-Hermitian skin effect via coherent coupling, *Phys. Rev. B* 106(8), 085427 (2022)
83. S. Mu, L. Zhou, L. Li, and J. Gong, Non-Hermitian pseudo mobility edge in a coupled chain system, *Phys. Rev. B* 105(20), 205402 (2022)
84. X. Zhang, C. Wu, M. Yan, and G. Chen, Observation of non-Hermitian pseudo-mobility-edge in a coupled electric circuit ladder, *Phys. Rev. B* 111(1), 014304 (2025)
85. S. Rafi-Ul-Islam, Z. B. Siu, H. Sahin, C. H. Lee, and M. B. A. Jalil, System size dependent topological zero modes in coupled topolectrical chains, *Phys. Rev. B* 106(7), 075158 (2022)
86. L. Wang, Z. Wang, J. Liu, and S. Chen, Exact multiple complex mobility edges and quantum state engineering in coupled one-dimensional quasicrystals, *Phys. Rev. B* 112(10), 104207 (2025)
87. Y. Yi and Z. Yang, Anomalous scaling behavior of green's function in critical skin effects, *Phys. Rev. B* 112(17), 174303 (2025)
88. Z. B. Siu, S. M. Rafi-Ul-Islam, and M. B. A. Jalil, Critical non-Hermitian skin effect in a single closed non-Hermitian chain, Preprints at Research Square (2022)
89. Y. Yi, Critical non-Hermitian skin effect induced by boundary defects, *Phys. Rev. B* 111(14), 144307 (2025)
90. Y. Qin, Y. S. Ang, C. H. Lee, and L. Li, Many-body critical non-Hermitian skin effect, *Commun. Phys.* 9(1), 16 (2025)
91. A. J. Daley, Quantum trajectories and open many body quantum systems, *Adv. Phys.* 63(2), 77 (2014)
92. A. McDonald, R. Hanai, and A. A. Clerk, Nonequilibrium stationary states of quantum non-Hermitian lattice models, *Phys. Rev. B* 105(6), 064302 (2022)
93. M. Abbasi, W. Chen, M. Naghiloo, Y. N. Joglekar, and K. W. Murch, Topological quantum state control through exceptional-point proximity, *Phys. Rev. Lett.* 128(16), 160401 (2022)
94. Y. X. Wang and A. A. Clerk, Non-Hermitian dynamics without dissipation in quantum systems, *Phys. Rev. A* 99(6), 063834 (2019)
95. A. McDonald, T. Pereg-Barnea, and A. A. Clerk, Phase-dependent chiral transport and effective non-Hermitian dynamics in a bosonic Kitaev–Majorana chain, *Phys. Rev. X* 8(4), 041031 (2018)
96. V. P. Flynn, E. Cobanera, and L. Viola, Deconstructing effective non-Hermitian dynamics in quadratic bosonic Hamiltonians, *New J. Phys.* 22(8), 083004 (2020)
97. Q. Wang, C. Zhu, Y. Wang, B. Zhang, and Y. D. Chong, Amplification of quantum signals by the non-

Hermitian skin effect, *Phys. Rev. B* 106(2), 024301 (2022)
98. N. Okuma, Boundary-dependent dynamical instability of bosonic Green's function: Dissipative Bogoliubov–de Gennes Hamiltonian and its application to non-Hermitian skin effect, *Phys. Rev. B* 105(22), 224301 (2022)
99. X. W. Luo, C. Zhang, and S. Du, Quantum squeezing and sensing with pseudo-anti-parity–time symmetry, *Phys. Rev. Lett.* 128(17), 173602 (2022)
100. V. P. Flynn, E. Cobanera, and L. Viola, Topology by dissipation: Majorana bosons in metastable quadratic Markovian dynamics, *Phys. Rev. Lett.* 127(24), 245701 (2021)
101. L. L. Wan and X. Y. Lü, Quantum-squeezing-induced point-gap topology and skin effect, *Phys. Rev. Lett.* 130(20), 203605 (2023)
102. K. Yokomizo and S. Murakami, Non-Bloch band theory in bosonic Bogoliubov–de Gennes systems, *Phys. Rev. B* 103(16), 165123 (2021)
103. C. C. Wanjura, M. Brunelli, and A. Nunnenkamp, Topological framework for directional amplification in driven-dissipative cavity arrays, *Nat. Commun.* 11(1), 3149 (2020)
104. S. Lieu, Topological symmetry classes for non-Hermitian models and connections to the bosonic Bogoliubov–de Gennes equation, *Phys. Rev. B* 98(11), 115135 (2018)
105. Z. Yang, Non-perturbative breakdown of Bloch's theorem and Hermitian skin effects, arXiv: 2012.03333 (2020)
106. O. Arandes and E. J. Bergholtz, Quantum sensing with driven-dissipative Su–Schrieffer–Heeger lattices, *Phys. Rev. Res.* 7(1), 013309 (2025)
107. K. B. Estake, T. R. Vishnu, and D. Roy, From chiral topological dynamics to chiral topological amplification: Real versus imaginary parameters in a Hermitian bosonic chain, *Phys. Rev. B* 112(21), 214314 (2025)
108. M. Bestler, A. Dikopoltsev, and O. Zilberberg, Non-Hermitian topology and skin modes in the continuum via parametric processes, arXiv: 2505.02776 (2025)
109. J. J. Slim, C. C. Wanjura, M. Brunelli, J. del Pino, A. Nunnenkamp, and E. Verhagen, Optomechanical realization of the bosonic Kitaev chain, *Nature* 627(8005), 767 (2024)
110. A. Pocklington, Y. X. Wang, and A. A. Clerk, Dissipative pairing interactions: Quantum instabilities, topological light, and volume-law entanglement, *Phys. Rev. Lett.* 130(12), 123602 (2023)
111. V. D. Vaidya, B. Morrison, L. G. Helt, R. Shahrokshahi, D. H. Mahler, M. J. Collins, K. Tan, J. Lavoie, A. Repingon, M. Menotti, N. Quesada, R. C. Pooser, A. E. Lita, T. Gerrits, S. W. Nam, and Z. Vernon, Broadband quadrature-squeezed vacuum and nonclassical photon number correlations from a nanophotonic device, *Sci. Adv.* 6(39), eaba9186 (2020)
112. R. Nehra, R. Sekine, L. Ledezma, Q. Guo, R. M. Gray, A. Roy, and A. Marandi, Few-cycle vacuum squeezing in nanophotonics, *Science* 377(6612), 1333 (2022)
113. A. H. Safavi-Naeini, S. Gröblacher, J. T. Hill, J. Chan, M. Aspelmeyer, and O. Painter, Squeezed light from a silicon micromechanical resonator, *Nature* 500(7461), 185 (2013)
114. J. del Pino, J. J. Slim, and E. Verhagen, Non-Hermitian chiral phononics through optomechanically induced squeezing, *Nature* 606(7912), 82 (2022)
115. S. Marti, U. von Lüpke, O. Joshi, Y. Yang, M. Bild, A. Omahen, Y. Chu, and M. Fadel, Quantum squeezing in a nonlinear mechanical oscillator, *Nat. Phys.* 20(9), 1448 (2024)
116. F. Lecocq, L. Ranzani, G. A. Peterson, K. Cicak, R. W. Simmonds, J. D. Teufel, and J. Aumentado, Nonreciprocal microwave signal processing with a field-programmable Josephson amplifier, *Phys. Rev. Appl.* 7(2), 024028 (2017)
117. B. Abdo, A. Kamal, and M. Devoret, Nondegenerate three-wave mixing with the Josephson ring modulator, *Phys. Rev. B* 87(1), 014508 (2013)
118. J. H. Busnaina, Z. Shi, A. McDonald, D. Dubyna, I. Nsanzineza, J. S. C. Hung, C. W. S. Chang, A. A. Clerk, and C. M. Wilson, Quantum simulation of the bosonic Kitaev chain, *Nat. Commun.* 15(1), 3065 (2024)
119. M. Villiers, W. C. Smith, A. Petrescu, A. Borgognoni, M. Delbecq, A. Sarlette, M. Mirrahimi, P. Campagne-Ibarcq, T. Kontos, and Z. Leghtas, Dynamically enhancing qubit-photon interactions with antisqueezing, *PRX Quantum* 5(2), 020306 (2024)